Photoionization of homonuclear diatomic molecules aligned by an intense femtosecond laser pulse

Masaaki Tsubouchi and Toshinori Suzuki*
Chemical Dynamics Laboratory, RIKEN, Wako 351-0198, Japan
(Received 31 January 2005; published 23 August 2005)

We calculated the photoelectron angular distribution (PAD) expected in the laboratory frame (LF PAD) for the ionization of N_2 molecules that are aligned by an intense laser pulse. We consider two independent processes of the dynamical alignment of molecules in the electronic ground state by an intense femtosecond laser pulse (>10 TW/cm^2) and one-photon ionization or (2+1) resonance-enhanced multiphoton ionization of the aligned molecules by a weak laser pulse (<10 GW/cm^2). We examined the variation of the LF PAD against the intensity of the alignment laser, durations of the alignment and ionization laser pulses, and the time delay between these pulses. The LF PAD obtained from the ionization of the aligned ensemble shows a semiquantitative agreement with the PAD in the molecular frame.

DOI: 10.1103/PhysRevA.72.022512 PACS number(s): 33.60.Cv, 42.50.Hz, 42.50.Md

I. INTRODUCTION

The photoelectron angular distribution (PAD) contains information on the phases of the photoelectron partial waves, and it serves as the most sensitive probe of photoionization dynamics. However, the PAD observed in the laboratory frame (LF) is typically a highly averaged quantity, which is achieved at the instant of ionization, obtained over the molecular axis distribution of the molecular frame (MF) PAD. Therefore the LF PAD is significantly less structured than the MF PAD. In order to overcome such difficulties and to extract information on photoionization dynamics, attempts have been made to observe the LF PAD for molecules whose axes are aligned or oriented in space. The photoion-photoelectron coincidence [1–6] is the most common technique employed to measure the relative angle between the photoelectron wave vector $\boldsymbol{k}$ and the vector $\boldsymbol{k}$ of the daughter ion in the axial recoil limit after dissociative ionization. The drawback of this technique is that it requires instantaneous dissociation of a molecular cation.

In the present paper, an alternative approach considered involves the preparation of an aligned ensemble of molecules prior to ionization. It should be noted that since the electrons are susceptible to electromagnetic fields, the alignment field should be absent at the instant of photoionization. Therefore the pendular states [7–11] created in the presence of an electric field are unsuitable for photoelectron spectroscopy. When the electromagnetic field is switched slower than the molecular rotational period, the rotational dynamics are generally adiabatic, and the overall alignment vanishes as the field disappears. In the special case demonstrated by a hexapole state selector, the static field is capable of allowing the transmission of molecules with particular (J,m_J) quantum numbers from an isotropic ensemble, thereby forming a weakly oriented ensemble. Kaesdorf *et al.* have demonstrated the application of the hexapole state selector to photoionization [12]. On the other hand, when the electromagnetic field is switched considerably faster than the molecular rotational period, the dynamics become nonadiabatic and the alignment is maintained even after the disappearance of the field. This alignment is induced by the quantum interference of field-free rotational wave functions that are combined by an instantaneous electromagnetic field. Previous studies have shown that an intense femtosecond laser pulse can create a superposition of field-free rotational states for the duration of the laser pulse and leaves the superposition state in the field-free space. It is interesting to note that the induced alignment may become stronger after the laser field is switched off [13]. The strength of the induced alignment is reasonably high, as shown previously by the directional ejection of daughter ions in multielectron dissociative ionization (MEDI) (or laser-induced Coulomb explosion) with intense femtosecond pulses [14–21].

In this paper, we consider the nonadiabatic rotational dynamics of homonuclear diatomic molecules in an intense laser field and the photoionization of this aligned ensemble of molecules. The nonadiabatic dynamical alignment has been considered theoretically for both the resonant [22,23] and nonresonant [13,24,25] cases. The signature of the rotational wave-packet motion has been observed experimentally for I_2 [17–19], N_2 [20,21], and O_2 [21] in the angular distributions of fragments and for CS_2 [26], CO_2 [26], acetylene [26], benzene [26], and iodobenzene [27] in the transient grating signals. This paper focuses on the examination of the PAD measurement for a laser-aligned ensemble of molecules. A schematic experimental diagram considered in this study is shown in Fig. 1. The first intense laser pulse creates a dynamical alignment of N_2 molecules. This results in the formation of a rotational wave packet in the electronic ground state. A second pulse of a different color ionizes these molecules when they are maximally aligned. For the ionization step, we consider (i) one-photon ionization and (ii) one-color (2+1) resonance-enhanced multiphoton ionization (REMPI).

II. THEORY

Two distinct optical processes are considered in order to observe the LF PAD in ionization of the aligned ensemble of

*Corresponding author: Email address: toshisuzuki@riken.jp

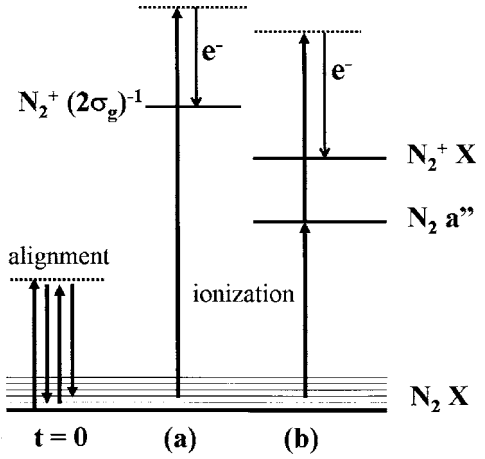

FIG. 1. Schematic diagram of the alignment and (a) one-photon ionization and (b) one-color (2+1) resonance-enhanced multiphoton ionization schemes of N_2.

molecules. One process is the dynamical alignment of molecules in the electronic ground state by nonperturbative interaction with an intense laser field (>10 TW/cm^2), and the other is one-photon ionization or (2+1) REMPI of these molecules by perturbative interaction with a moderate laser field (<10 GW/cm^2). We will use three different angles in the following discussion: the angles with no subscripts $\{\theta, \phi, \Omega\}$ correspond to those of the molecular axis considered with respect to the laboratory frame, and those with the subscript LF or MF correspond to the photoelectron wave vector $\boldsymbol{k}$ in the LF or MF, respectively.

A. Molecular axis alignment and its time evolution

1. Hamiltonian

We consider a homonuclear diatomic molecule with zero electronic angular momentum and polarizability components that are parallel ($\alpha_\parallel$) and perpendicular ($\alpha_\perp$) to the axis. The nonresonant interaction between the molecule and the laser field $\varepsilon(t)$ is described by the following Hamiltonian [7,24,28,29]:

$$\hat{H}(t) = B\mathbf{J}^2 - \frac{1}{2}\varepsilon^2(t)[(\alpha_\parallel - \alpha_\perp)\cos^2\theta + \alpha_\perp], \tag{1}$$

where B is the rotational constant, $\mathbf{J}^2$ is the squared angular momentum operator, and θ is the polar angle between the molecular axis and the electric vector of the linearly polarized light. The time-dependent laser field with an amplitude E_0 and a frequency ν is written as

$$\varepsilon(t) = \sqrt{g(t)}E_0\cos(2\pi\nu t), \tag{2}$$

where $g(t)$ is a dimensionless normalized time profile of the laser field that was postulated to be a Gaussian function with a full width at half maximum (FWHM) of Δt_{align}.

The practical form of the Hamiltonian in units of cm^{-1} becomes

$$\hat{H}(t) = B\mathbf{J}^2 - f(t)[(\Delta\alpha')\cos^2\theta + \alpha'_\perp], \tag{3}$$

where $f(t) = 10.553\ g(t)I\cos^2(2\pi\nu t)$ and $\Delta\alpha' = \alpha'_\parallel - \alpha'_\perp$. I represents the laser intensity in W/cm^2 and α' represent the volume polarizabilities in Å^3.

2. Rotational wave packet

The time-dependent rotational wave function $\Psi(t)$ (rotational wave packet) can be expanded in terms of the spherical harmonics of $|jm\rangle \equiv Y_{jm}(\theta, \phi)$ as follows:

$$\Psi(t) = \sum_{jm} C_{jm}(t)|jm\rangle, \tag{4}$$

where j is the total angular momentum quantum number, and m is the projection quantum number of j on the space fixed axis. The time-dependent Schrödinger equation obtained using Eqs. (3) and (4) provides the following differential equations of the coefficients $C_{jm}(t)$:

$$\begin{aligned} i\hbar\frac{\partial C_{jm}(t)}{\partial t} = {} & C_{jm}(t)[Bj(j+1) - f(t)\alpha'_\perp] - f(t)\Delta\alpha'[C_{j-2,m}(t) \\ & \times\langle jm|\cos^2\theta|j-2,m\rangle + C_{jm}(t)\langle jm|\cos^2\theta|jm\rangle \\ & + C_{j+2,m}(t)\langle jm|\cos^2\theta|j+2,m\rangle]. \end{aligned} \tag{5}$$

The matrix elements are

$$\langle jm|\cos^2\theta|j-2,m\rangle = \frac{1}{2j-1}\sqrt{\frac{(j^2-m^2)\{(j-1)^2-m^2\}}{(2j+1)(2j-3)}}, \tag{6a}$$

$$\langle jm|\cos^2\theta|jm\rangle = \frac{1}{3} + \frac{2}{3}\frac{j(j+1)-3m^2}{(2j+3)(2j-1)}, \tag{6b}$$

and

$$\langle jm|\cos^2\theta|j+2,m\rangle = \frac{1}{2j+3}\sqrt{\frac{\{(j+2)^2-m^2\}\{(j+1)^2-m^2\}}{(2j+5)(2j+1)}}. \tag{6c}$$

The differential equation (5) indicates that the molecular axis alignment is due to multiple Raman processes. Since the rotational selection rule of a single Raman process is $\Delta j = 0, \pm 2$, and $\Delta m = 0$, rotational states with same parities and m are coupled to each other in the laser field. Therefore when the expansion of Eq. (4) is truncated at $j = j_{\max}$, the series of differential equations is divided into $4j_{\max}$ $[=2j_{\max}+1+2(j_{\max}-1)+1]$ sets of the equation.

The time-dependent distribution function of the molecular axis is written as

$$P(\theta;t) = \int\int d\phi d\chi \Psi(t)\Psi^*(t)$$
$$= \int\int d\phi d\chi \sum_m \left[\sum_{\substack{\text{even } j_1 \\ \text{even } j_2}} C_{j_1 m}(t) C^*_{j_2 m}(t) \times Y_{j_1 m}(\theta,\phi) Y^*_{j_2 m}(\theta,\phi) + \sum_{\substack{\text{odd } j_1 \\ \text{odd } j_2}} C_{j_1 m}(t) C^*_{j_2 m}(t) Y_{j_1 m}(\theta,\phi) Y^*_{j_2 m}(\theta,\phi) \right], \tag{7}$$

It may also be represented by the expectation value of $\cos^2\theta$:

$$\langle \cos^2\theta \rangle = \frac{\int \sin\theta d\theta \cos^2\theta P(\theta;t)}{\int \sin\theta d\theta P(\theta;t)}. \tag{8}$$

The value of $\langle \cos^2\theta \rangle$ ranges from 1 (all molecular axes are aligned parallel to the laser polarization vector) to 0 (perpendicular), and it takes the values of 3/5, 1/3, and 1/5 for $\cos^2\theta$, isotropic, and $\sin^2\theta$ distributions, respectively.

B. Two-photon excitation of the aligned ensemble

In one-color (2+1) REMPI, the rotational wave packet in the electronic ground state is transferred to the excited state due to the two-photon absorption of the ionization light. We consider the ${}^1\Sigma_g \leftarrow\leftarrow {}^1\Sigma_g$ two-photon transition of a homonuclear diatomic molecule. Further, we assume that the polarization of the ionization light is parallel to that of the alignment light. When the molecules are excited at the delay time t after the application of the alignment pulse, the rotational wave packet in the excited states is described as

$$\Psi'(t) = \sum_{j''m''} C_{j''m''}(t) \sum_{j'm'} F(j'm';j''m'') |j'm'\rangle, \tag{9}$$

where $|j''m''\rangle$ and $|j'm'\rangle$ are the rotational eigenfunctions in the electronic ground states and excited states, respectively. $F(j'm';j''m'')$ is the two-photon transition-matrix element for the $|{}^1\Sigma_g\rangle|j'm'\rangle \leftarrow\leftarrow |{}^1\Sigma_g\rangle|j''m''\rangle$ process provided by [30]

$$F(j'm';j''m'') \propto (-1)^{m''}\sqrt{(2j'+1)(2j''+1)} \times \left\{ (1-\gamma) \begin{pmatrix} j' & j'' & 0 \\ m' & -m'' & 0 \end{pmatrix} \begin{pmatrix} j' & j'' & 0 \\ 0 & 0 & 0 \end{pmatrix} + \sqrt{10}\left(1+\frac{\gamma}{2}\right) \begin{pmatrix} j' & j'' & 2 \\ m' & -m'' & 0 \end{pmatrix} \begin{pmatrix} j' & j'' & 2 \\ 0 & 0 & 0 \end{pmatrix} \right\}. \tag{10}$$

Here, γ is the ratio of the transitions *via* the Π and Σ virtual states and is related to the transition path ratio μ_I/μ_S by Bray and Hochstrasser [31] as follows:

$$\left(\frac{\mu_I}{\mu_S}\right)^2 = \frac{1}{5}\left(\frac{1-\gamma}{2+\gamma}\right)^2. \tag{11}$$

The distribution function of the molecular axes in the excited state is calculated by $P'(\theta;t) = \int\int d\phi d\chi \Psi'(t)\Psi'^*(t)$.

C. Photoelectron angular distribution

In the photoionization of a diatomic molecule, the photoelectron scattering wave function in the molecular frame (MF) can be expanded into partial waves of spherical harmonics [32] as follows:

$$|\psi^-(\vec{k}_{MF},\vec{r})\rangle = \sum_l i^l \exp(-i\sigma_l) \sum_\lambda Y^*_{l\lambda}(\hat{k}_{MF}) \varphi_{l\lambda}(k_{MF},\vec{r}), \tag{12}$$

where $\vec{k}_{MF}$ and $\vec{r}$ are the wave and position vectors of the photoelectron in the MF, respectively; l and λ are the quantum numbers of the orbital angular momentum and its projection onto the molecular axis, respectively; σ_l is the Coulomb phase shift; and $\varphi_{l\lambda}(k_{MF},\vec{r})$ is the partial wave. The MF PAD with linearly polarized ionization light is written as [32,33]

$$I(\theta_{MF},\phi_{MF}) = |\langle \Psi^+;\psi^-(\vec{k}_{MF},\vec{r})|\vec{\mu}\cdot\vec{\varepsilon}|\Psi^i\rangle|^2 = \sum_{LM} B_{LM} Y_{LM}(\theta_{MF},\phi_{MF}), \tag{13}$$

where $\vec{\mu}\cdot\vec{\varepsilon} = \Sigma_\lambda D^1_{0\lambda}{}^*(\Omega)\mu_\lambda$ is the scalar product of the ionization dipole moment and the electric vector of the ionization laser in the MF; Ψ^+ and Ψ^i are the wave functions of the cation and the ionized states, respectively; θ_{MF} and ϕ_{MF} are the polar and azimuthal angles of the photoelectron wave vector $\boldsymbol{k}$ with respect to the internuclear axis, respectively; $D^1_{0\lambda}(\Omega)$ is the Wigner rotation matrix element [34], and Ω is the Euler angle of the MF with respect to the LF. B_{LM} is given by

$$B_{LM} = \sqrt{\frac{2L+1}{4\pi}} \sum_P (2P+1) \begin{pmatrix} 1 & 1 & P \\ 0 & 0 & 0 \end{pmatrix} \sum_{ll'} \sqrt{(2l+1)(2l'+1)} \times \begin{pmatrix} l & l' & L \\ 0 & 0 & 0 \end{pmatrix} \sum_{\lambda\lambda'} \begin{pmatrix} 1 & 1 & P \\ \lambda & -\lambda' & \lambda'-\lambda \end{pmatrix} \times \begin{pmatrix} l & l' & L \\ \lambda & -\lambda' & M \end{pmatrix} D^P_{0,\lambda'-\lambda}(\Omega)(-i)^{l-l'} \exp\{i(\sigma_l-\sigma_{l'})\} \times \exp\{i(\tau_{l\lambda}-\tau_{l'\lambda'})\} d_{l\lambda} d_{l'\lambda'}, \tag{14}$$

where $\tau_{l\lambda} = \arg(\langle \Psi^+;\varphi_{l\lambda}(k_{MF},\vec{r})|\mu_\lambda|\Psi^i\rangle)$ is the short-range scattering phase shift, $d_{l\lambda} = |\langle \Psi^+;\varphi_{l\lambda}(k_{MF},\vec{r})|\mu_\lambda|\Psi^i\rangle|$ is the magnitude of the transition dipole matrix element between the ionized orbital and the photoelectron partial wave, and P is a summation index. We define the total phase shift as $\delta_{l\lambda} = \sigma_l + \tau_{l\lambda}$.

The experimentally observed LF PAD corresponds to the average of the MF PAD for the molecular axis distribution in space. Therefore the analytical form of the LF PAD is expressed as [33,35]

$$I(\theta_{\mathrm{LF}},\phi_{\mathrm{LF}};t) = \int d\Omega P(\theta;t)\sum_{LQ}\left(\sum_{M} B_{LM}D^{L}_{QM}{}^{*}(\Omega)\right)Y_{LQ}(\theta_{\mathrm{LF}},\phi_{\mathrm{LF}}) = \sum_{LQ}\beta_{LQ}(t)Y_{LQ}(\theta_{\mathrm{LF}},\phi_{\mathrm{LF}}), \quad (15)$$

where θ_{LF} and ϕ_{LF} are the respective polar and azimuthal angles of the photoelectron wave vector $\boldsymbol{k}$ with respect to the polarization of the ionization laser, and

$$\beta_{LQ}(t) = \sqrt{\frac{2L+1}{4\pi}}\sum_{P}(2P+1) \times \begin{pmatrix} 1 & 1 & P \\ 0 & 0 & 0 \end{pmatrix}\sum_{ll'}\sqrt{(2l+1)(2l'+1)}\begin{pmatrix} l & l' & L \\ 0 & 0 & 0 \end{pmatrix} \times \sum_{\lambda\lambda'}\begin{pmatrix} 1 & 1 & P \\ \lambda & -\lambda' & \lambda'-\lambda \end{pmatrix}(-i)^{l-l'} \times \exp\{i(\delta_{l\lambda}-\delta_{l'\lambda'})\}d_{l\lambda}d_{l'\lambda'}\sum_{M}\begin{pmatrix} l & l' & L \\ \lambda & -\lambda' & M \end{pmatrix} \times \int d\Omega P(\theta;t)D^{P}_{0,\lambda'-\lambda}(\Omega)D^{L}_{QM}{}^{*}(\Omega). \quad (16)$$

Once we obtain a complete set of the dynamical parameters of ionization $d_{l\lambda}$ and $\delta_{l\lambda}$, Eqs. (13)–(16) provide the MF and LF PADs.

III. RESUTS AND DISCUSSION

In this section, we calculate the molecular axis alignment and photoionization of N_2 by using femtosecond laser light. First, the time-dependent molecular axis alignment in the $X\ {}^1\Sigma_g{}^+$ state and its dependence on laser intensity (I) and pulse width ($\Delta t_{\mathrm{align}}$) of the alignment are examined. Next, the LF PAD ionized from the excited electronic state into the $N_2{}^+$ continuum using a femtosecond probe pulse is compared with the MF PAD.

A. Molecular axis alignment in the X state

Figure 2 shows the calculated time-dependent rotational state distributions, $P(j)=\Sigma_m|C_{jm}(t)|^2$, in the X state arising from the interaction with an intense nonresonant femtosecond laser pulse (800 nm) with intensity $I=100$ TW/cm^2 and duration $\Delta t_{\mathrm{align}}=100$ fs. The integration of the differential equations (5) was facilitated by the fourth-order Runge-Kutta method with time steps of 0.1 fs and a maximum rotational quantum number of $j_{\max}=20$. (These conditions are constant throughout this paper.) We used the rotational and centrifugal constants of $B_0''=1.9896$ cm^{-1} and $D_0''=5.76\times10^{-6}$ cm^{-1} [36] and the volume polarizabilities of $\alpha_{\parallel}=2.38$ Å^3 and $\alpha_{\perp}=1.45$ Å^3 [37] in the ground electronic state. We assumed the initial rotational distribution to be a single state of $|j=0,m=0\rangle$ and the Boltzmann distribution at the rotational temperature $T_{\mathrm{R}}=20$ K for the calculations shown in Figs. 2(a) and 2(b), respectively. For the latter, the 2:1 relative abundances of ortho- and para-N_2 were also considered; ortho and para correspond to the total nuclear spin states of $T=0$ and 2 and $T=1$, respectively [38]. Due to the selection rule of the rotational Raman scattering, the rotational states with even and odd values of j evolve independently; therefore Fig. 2(b) is divided into two sections for the even and odd j states. Beginning from the $|j=0,m=0\rangle$ state in Fig. 2(a), the states $j=2$, 4, and 6 emerge successively in ~30 fs. After the interaction with the laser field, the molecules populate up to $j=12$ with a maxima at $j=6$ or 8. On the other hand, at T_{R}

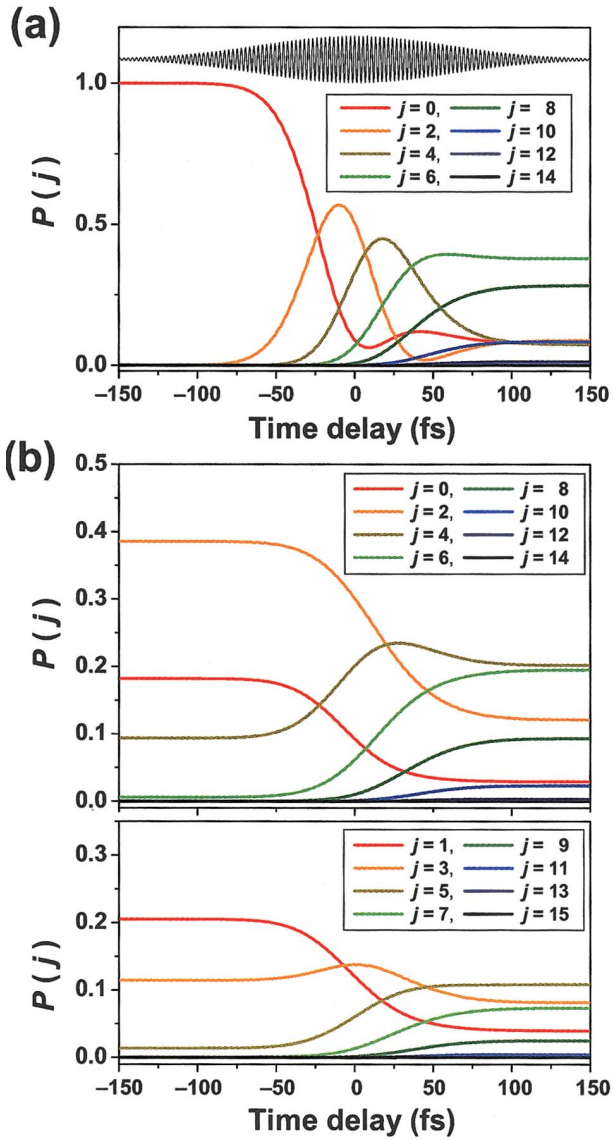

FIG. 2. (Color) Time evolution of the rotational state population, $P(j)=\Sigma_m|C_{jm}(t)|^2$. The intensity and pulse width of the alignment laser light in the calculation are $I=100$ TW/cm^2 and $\Delta t_{\mathrm{align}}=100$ fs, respectively. The initial rotational temperatures are (a) $T_{\mathrm{R}}=0$ K with only $|j=0,m=0\rangle$ as an initial state and (b) 20 K (molecular-beam condition). The time profile of the laser field amplitude $\varepsilon(t)$ is also shown in (a).

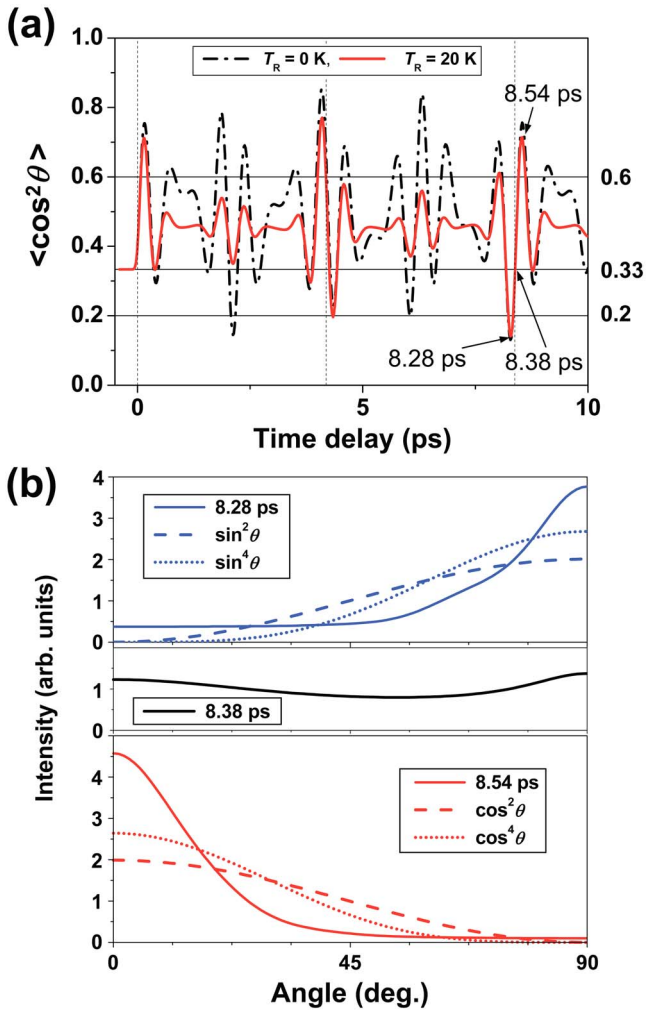

FIG. 3. (Color online) (a) Time evolution of the expectation value $\langle\cos^2\theta\rangle$. The intensity and pulse width of the alignment laser light in the calculation are $I=100$ TW/cm^2 and $\Delta t_{\text{align}}=100$ fs, respectively. The initial rotational temperatures are $T_R=0$ K (black) and 20 K (red). The full revival time of the rotational wave packet in the X state of N_2 is 8.38 ps. The axis distribution becomes isotropic $\langle\cos^2\theta\rangle=1/3$ at the full revival time of 8.38 ps. The horizontal dotted lines represent $\langle\cos^2\theta\rangle=3/5$, $1/3$, and $1/5$ corresponding to the axis distributions of $P(\theta)\propto\cos^2\theta$, 1, and $\sin^2\theta$, respectively. (b) Molecular axis distributions $P(\theta;t)$ at the mentioned time delays. The $\cos^n\theta$ and $\sin^n\theta$ functions are also shown in the figure for comparison.

=20 K, the molecules initially distribute over the rotational states of $j=0-4$ with the maxima at $j=2$, and spread more widely over the $j=2-10$ states after the interaction with the laser radiation.

The time evolution of the expectation value of $\langle\cos^2\theta\rangle$ is shown in Fig. 3(a). The value was calculated using the time-dependent molecular axis distribution $P(\theta;t)$ shown later in Fig. 4. Figure 3(a) shows $\langle\cos^2\theta\rangle$ up to the first revival time of $\tau=1/2cB_0''=8.38$ ps. The features at the quarter and three quarter revivals diminish at 20 K in comparison with those at 0 K because of incoherent summation over the initial rotational states. Near the full revival time of 8.38 ps, the molecular axis alignment rapidly changes within only 0.3 ps;

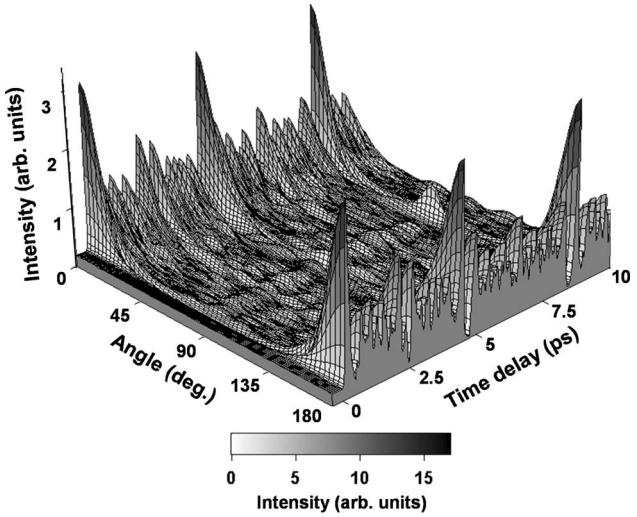

FIG. 4. Time-dependent molecular axis distribution $P(\theta;t)$ in the X state calculated at $T_R=20$ K. The intensity and pulse width of the alignment laser light in the calculation are $I=100$ TW/cm^2 and $\Delta t_{\text{align}}=100$ fs, respectively. The angular distributions are normalized as $\int\sin\theta d\theta P(\theta;t)=1$.

the maximal and minimal values of $\langle\cos^2\theta\rangle$ at 20 K are 0.71 and 0.14 at 8.54 and 8.28 ps, respectively. The axis distribution becomes isotropic ($\langle\cos^2\theta\rangle=1/3$) at the full revival time of 8.38 ps. These values are compared with $\langle\cos^2\theta\rangle=0.6$ and 0.2 that are expected for the molecular axis distributions of $P(\theta)=\cos^2\theta$ or $\sin^2\theta$, respectively, which indicate the maximal alignment created by a one-photon dipole transition. The alignment in the ground electronic state induced by an intense femtosecond laser field is considerably stronger than that induced by the one-photon absorption process.

In Fig. 3(b), the molecular axis distributions $P(\theta;t)$ at the mentioned time delays are compared with the functions $\sin^n\theta$ and $\cos^n\theta$ ($n=2$ and 4). The molecular axis distribution at 8.54 ps with the maximal alignment is considerably sharper than $\cos^4\theta$ and is well fitted to the function of $\cos^{15}\theta$ with a FWHM of 31°, which may be compared with 90° and 66° for the distributions of $\cos^2\theta$ and $\cos^4\theta$, respectively.

Figure 4 shows the time-dependent molecular axis distribution $P(\theta;t)$ calculated for $T_R=20$ K. The angular distributions are normalized as $\int\sin\theta d\theta P(\theta;t)=1$. The distribution rapidly changes in time and has a complex structure with several nodes.

Figure 5(a) shows the dependence of the final rotational state distribution on the laser intensity (I) after the interaction with the alignment pulse of $\Delta t_{\text{align}}=100$ fs at $T_R=20$ K. As the peak intensity of the laser pulse is increased from 25 to 200 TW/cm^2, the distribution spreads and the peak value of j progressively shifts to the right. The intensity alternation in the distribution is due to the relative abundance of ortho- and para-N_2. The time evolutions of the alignment parameter $\langle\cos^2\theta\rangle$ are shown in Fig. 6(a). At the full revival time of 8.38 ps, the distribution is always isotropic ($\langle\cos^2\theta\rangle=1/3$), and the time derivative of $\langle\cos^2\theta\rangle$ is positive. The variation of the alignment parameter becomes

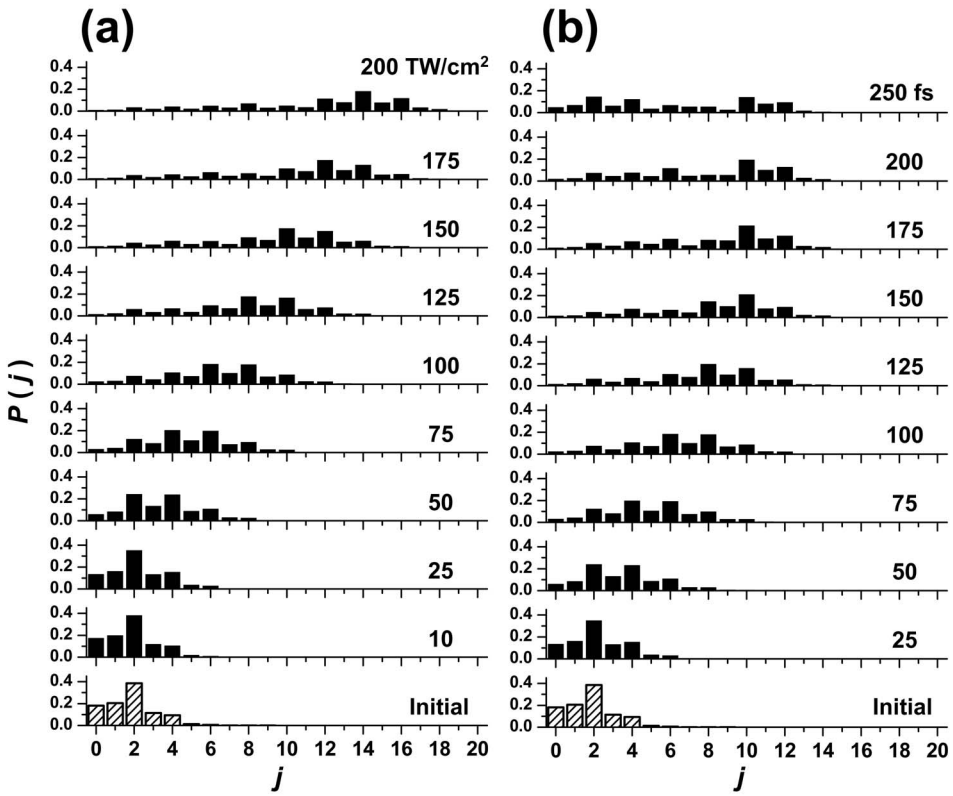

FIG. 5. Final rotational state distributions in the X state after the interaction with the alignment pulse. The initial rotational temperature of the sample in the calculation is $T_R=20$ K. (a) Dependence on the laser intensity I at the fixed pulse width of $\Delta t_{align}=100$ fs and (b) dependence on the pulse width Δt_{align} at the fixed laser intensity $I=100$ TW/cm^2.

faster with an increase in the laser intensity. Dooley *et al.* have explained this trend in which the dominant frequency in the revival structure corresponds to the beat frequency between the most highly populated states $|j\rangle$ and $|j+2\rangle$ of the wave packet and that this frequency increases with the laser intensity [21]. The peak value of $\langle\cos^2\theta\rangle$ also increases monotonically with the alignment laser intensity. However, at an intensity greater than 150 TW/cm^2, the alignment parameter does not increase dramatically. Therefore we considered the value $I=100$ TW/cm^2 for the following calculations since a lower intensity of the alignment laser is preferable to suppress the nonresonant ionization process that might disturb the actual experiment.

Figures 5(b) and 6(b) show the dependence of the final rotational state distribution on the pulse width Δt_{align} and the time evolution of $\langle\cos^2\theta\rangle$, respectively, for $I=100$ TW/cm^2 and $T_R=20$ K. As the laser pulse width is increased from 25 to 150 fs, the peak value of j progressively shifts to the right. However, at a pulse width greater than 150 fs, the peak value of j ceases to shift, and the rotational state distribution widens. This suggests that the anti-Stokes Raman process of $|j\rangle \rightarrow |j-2\rangle$ is operative in the intense laser field with a longer time duration. The time evolution of $\langle\cos^2\theta\rangle$ shown in Fig. 6(b) exhibits a similar trend. At $\Delta t_{align}=150$ fs, the peak value of $\langle\cos^2\theta\rangle$ is maximum, while at $\Delta t_{align}>150$ fs, it diminishes with an increase in the pulse width. Thus the pulse width of 100 fs was employed in the following LF PAD calculations.

B. PAD in one-photon ionization obtained from the X state

Figure 7 shows the spherical plots of the MF PADs for the one-photon ionization of N_2 at $h\nu=58.2$ eV that are calcu-

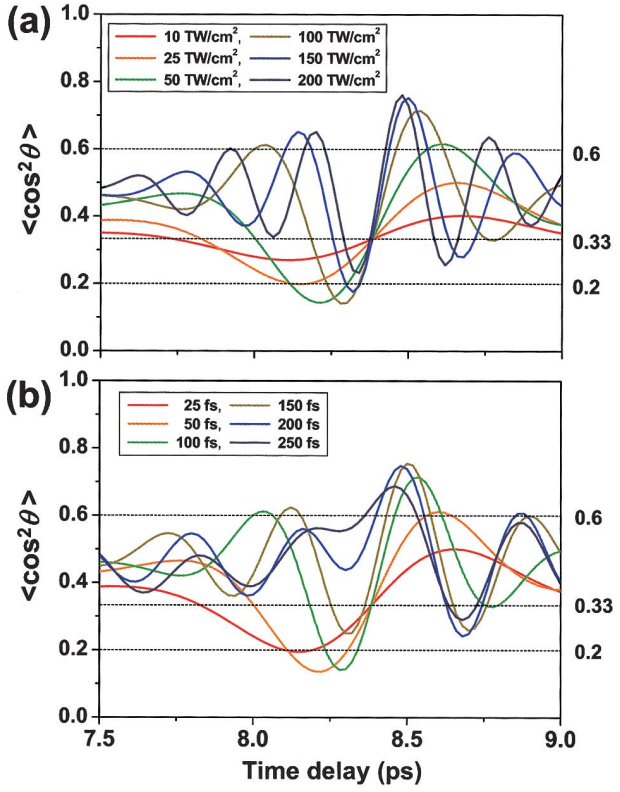

FIG. 6. (Color) Time evolution of the expectation value $\langle\cos^2\theta\rangle$ in the X state. The initial rotational temperature of the sample in the calculation is $T_R=20$ K. (a) Dependence on the laser intensity I at the fixed pulse width of $\Delta t_{align}=100$ fs and (b) dependence on the pulse width Δt_{align} at the fixed laser intensity $I=100$ TW/cm^2.

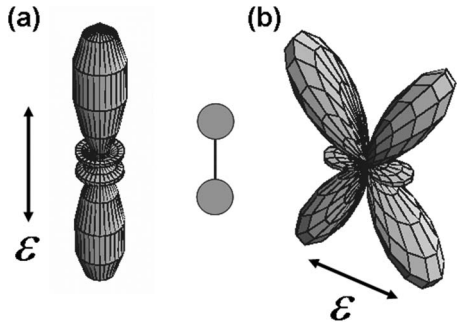

FIG. 7. Spherical plots of the MF PADs in the one-photon ionization of the X state of N_2. The internuclear axis is fixed vertically in the plane of the figure, and the linear polarizations of the ionization light are (a) parallel and (b) perpendicular to it. We used the dynamical parameters of ionization reported for the $2\sigma_g$-shell photoionization ($h\nu$=58.2 eV) [39,40].

lated using Eqs. (13) and (14). The internuclear axis is fixed vertically in the plane of the figure, and the linear polarization of the ionization light is (a) parallel and (b) perpendicular to the internuclear axis. We used the dynamical parameters of ionization derived from the experiments by Motoki *et al.* for the $2\sigma_g$-shell photoionization ($h\nu$=58.2 eV) [39,40]. The parameters used are listed in Table I. Only the photoelectron partial waves with the *ungerade* symmetry $(p,f,,\ldots)$ are allowed in one-photon ionization from the $2\sigma_g$ shell. In this study, we considered only the p and f partial waves for simplicity. The selection rule of $\Delta\lambda=0,\pm1$ also restricts the λ value of the outgoing wave to 0 and ±1. As shown in Table I, f waves are the main components of the PADs. The calculated MF PADs shown in Fig. 7 exhibit nodal patterns of the f waves, which are identical to those observed by Motoki *et al.* [39,40].

Figure 8(a) shows the polar plots of the LF PADs that are expected for the ionization of time-evolving aligned molecules near the full revival time. We assumed that the ionization light has a negligible pulse duration and that its polarization vector is parallel to that of the alignment laser light and vertical in the plane of the figure, as indicated by arrows. As shown in Fig. 3, the molecular axes at 8.28 and 8.54 ps are aligned such that they are highly perpendicular and parallel to the laser polarization. On the other hand, at the revival time of 8.38 ps, the molecules distribute isotropically in space. Therefore the LF PAD, shown in Fig. 8(a), strongly depends on the delay time between the alignment and the

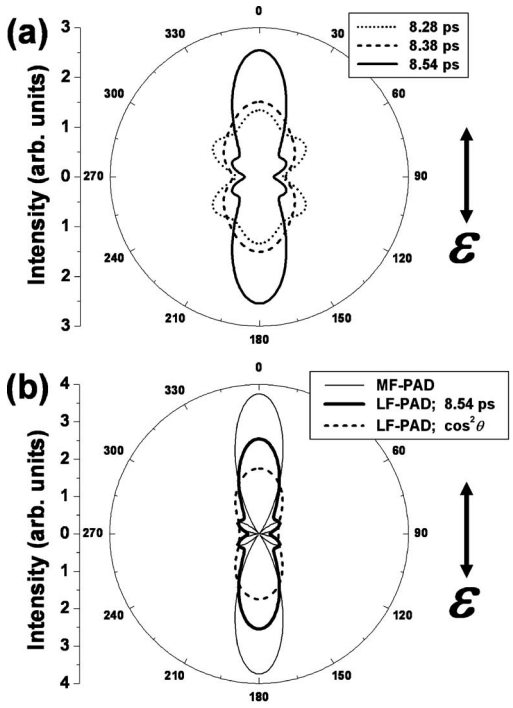

FIG. 8. Polar plots of the LF PADs in the one-photon ionization of the time-evolving aligned molecules. The ionization light is assumed to have an infinitely short pulse width, and its polarization vector is parallel to that of the alignment laser light and vertical in the plane of the figure. The initial rotational temperature of the sample in the calculation is T_R=20 K. The intensity and pulse width of the alignment laser light in the calculation are I=100 TW/cm^2 and Δt_{align}=100 fs, respectively. (a) LF PADs at different time delays. (b) comparison of the LF PAD with the MF PAD at the delay time of 8.54 ps. The LF PAD expected for the $\cos^2\theta$ axis distribution is also shown in this figure.

ionization pulses, that is, the molecular axis distribution in space. When the molecules are aligned parallel to the polarization vector, the nodal pattern of the MF PAD also appears in the LF PAD. A comparison between the LF PAD obtained at 8.54 ps and the MF PAD is shown in Fig. 8(b). The expected LF PAD for the ensemble with the $\cos^2\theta$ axis distribution is also shown in the figure for comparison. The LF PAD expected for the strongly aligned ensemble at 8.54 ps is not identical yet very similar to the MF PAD. Such a pattern is never obtained for the LF PAD from weakly aligned ensembles.

TABLE I. Dynamical parameters $d_{l\lambda}$ and $\delta_{l\lambda}$ of the photoionization of N_2 that were used in the calculation of the photoelectron angular distributions. Cases 1 and 2 correspond to the one-photon ionization of the $2\sigma_g$ orbital with $h\nu$=58.2 eV and $4\sigma_g$ orbital ($3s\sigma_g$ Rydberg) with light of 202.4 nm, respectively. The phase shift is expressed in radians.

	$d_{p\sigma}$	$d_{p\pi}$	$d_{f\sigma}$	$d_{f\pi}$	$\delta_{p\sigma}-\delta_{f\pi}$	$\delta_{p\pi}-\delta_{f\pi}$	$\delta_{f\sigma}-\delta_{f\pi}$
Case 1	0.35±0.08[a]	0.51±0.07[a]	1.79±0.22[a]	≡1	5.37±0.30[a]	2.06±0.09[a]	0.91±0.19[a]
Case 2	1.02[b]	0.89[b]	1.40[b]	≡1	3.22[c]	3.47[c]	0.0025[c]

[a]Ref. [39].
[b]These values are derived from Fig. 4 in Ref. [42].
[c]Phase shifts are derived from the quantum defects of the high Rydberg states of N_2 determined in Ref. [45].

The calculated LF PAD at the delay time of 8.28 ps is not similar to the MF PAD. This is because the molecular axis distribution generated by the linearly polarized alignment laser light is cylindrically symmetric with respect to the polarization, and the molecular axis at 8.28 ps is distributed in the plane perpendicular to the polarization. Therefore the molecular axis is not fixed in a particular direction in the LF. The observed LF PAD is thus averaged over the azimuthal axis distribution.

As mentioned in the last section, the angular distribution of the molecular axis generated by the intense femtosecond laser pulse varies rapidly in time. Therefore the LF PAD observed during the ionization of a rapidly moving rotational wave packet in the ground electronic state is affected by the finite pulse width of the laser. The normalized LF PADs are calculated using the following equation:

$$I(\theta_{\mathrm{LF}},\phi_{\mathrm{LF}};t)=\sum_{LQ}\left[\frac{\int dtg(t)\beta_{LQ}(t)}{\int dtg(t)}\right]Y_{LQ}(\theta_{\mathrm{LF}},\phi_{\mathrm{LF}})$$
$$=\sum_{LQ}\bar{\beta}_{LQ}(t)Y_{LQ}(\theta_{\mathrm{LF}},\phi_{\mathrm{LF}}), \quad (17)$$

where $g(t)$ is the time profile of the ionization pulse. Figures 9(a) and 9(b) show the dependence of the averaged anisotropy parameters $\bar{\beta}_{L0}/\bar{\beta}_{00}$ and the polar plots of the LF PADs on the ionization pulse width Δt_{ion} at the delay time of 8.54 ps, respectively. The longer pulse width of the ionization light reduces the anisotropy and blurs the nodal structure of the PAD. This suggests that the observation of the molecular alignment is hindered by the finite ionization pulse duration. In the previous study, the axis distributions observed experimentally were more isotropic than the calculated ones [21]. This discrepancy may be attributed to the probe pulse duration, although other effects (laser beam profile, ionization by the alignment pulse, etc.) cannot be ignored.

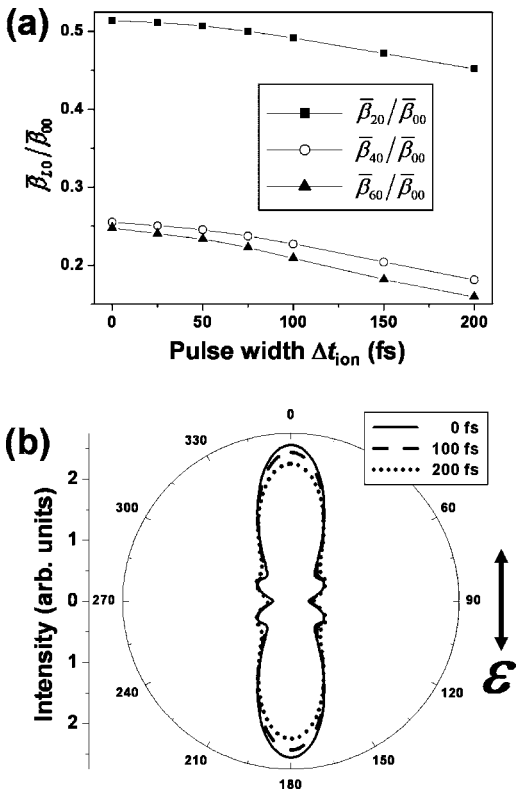

FIG. 9. Dependence of (a) the normalized anisotropy parameters $\bar{\beta}_{L0}/\bar{\beta}_{00}$ and (b) the LF PADs on the ionization pulse width Δt_{ion} at the delay time of 8.54 ps. The polarization vector of the ionization light is parallel to that of the alignment laser light and is vertical in the plane of the figure. The initial rotational temperature of the sample in the calculation is $T_{\mathrm{R}}=20$ K. The intensity and pulse width of the alignment laser light in the calculation are $I=100$ TW/cm^2 and $\Delta t_{\mathrm{align}}=100$ fs, respectively.

C. PAD in (2+1) REMPI via the a'' state

In the laser experiment, the REMPI scheme is widely used to ionize molecules. In this section, we calculate the LF PADs for one-color (2+1) REMPI of the aligned ensemble in the ground electronic state via the a'' state using 202.4 nm light. The polarization of the ionization light is assumed to be parallel to that of the alignment light. Photoelectrons with kinetic energies of 2.8 eV are generated in this ionization scheme.

1. Angular distribution in the a'' state

First, we consider the two-photon excitation process: $N_2(a'',{}^1\Sigma_g^+)\leftarrow\leftarrow N_2\ (X,{}^1\Sigma_g^+)$. For this transition, the virtual state path ratio $\mu_{\mathrm{I}}/\mu_{\mathrm{S}}=12.5\pm5$ has been obtained by Hanisco and Kummel from the measurements of the relative intensities of the O and Q branches [41]. The axis alignment of the molecules in the X state is projected onto the a'' state by the two-photon transition with the ionization light. This transition is induced by the perturbative dipole interaction with the ionization pulse. The time profiles of $\langle\cos^2\theta\rangle$ around the full revival time are shown in Fig. 10(a). The intensity and pulse width of the alignment laser light used in the calculation are $I=100$ TW/cm^2 and $\Delta t_{\mathrm{align}}=100$ fs, respectively. The dashed line represents the time evolution of the alignment parameter in the X state. The solid lines represent the alignment parameter in the a'' state that depends on the time delay between the alignment and the ionization laser pulse. Since the transition $a''\leftarrow\leftarrow X$ is parallel to the molecular axis, the alignment in the a'' state is more enhanced than that in the X state.

Figure 10(b) shows the molecular axis distributions $P(\theta;t)$ in the a'' state generated at 8.54 ps when maximal alignment is achieved with the polarization axis of the alignment laser in the X state. The angular distribution in the X state at 8.54 ps indicated by a dashed line is also shown for comparison. In the X state, the small number of molecules still direct their axis perpendicular to the laser polarization ($\theta=60°-90°$). On the other hand, such molecules do not contribute to the angular distribution in the a'' state. Although the angular anisotropy is fairly reduced because of the finite duration of the laser pulse for REMPI, the alignment parameter $\langle\cos^2\theta\rangle$ is clearly higher than that in the X state. The axis distributions in the a'' state that are excited by

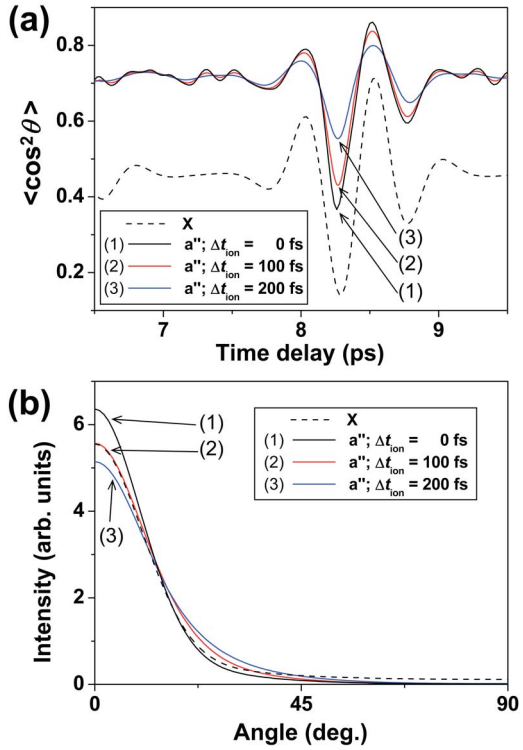

FIG. 10. (Color online) (a) Time profiles of the alignment parameter $\langle \cos^2 \theta \rangle$ around the full revival time. The dashed line represents the alignment parameter in the X state. The solid lines represent the alignment parameter in the a'' state that is excited by the two-photon transition from the aligned X state. (b) Molecular axis distributions $P(\theta;t)$ in the a'' state generated at the time delay of 8.54 ps when maximal alignment is achieved in the X state. The simultaneous distribution in the X state is also shown by the dashed line for comparison. The dependence on the ionization pulse width Δt_{ion} is shown in both (a) and (b). The initial rotational temperature of the sample in the calculation is $T_{\text{R}}=20$ K. The intensity and pulse width of the alignment laser light in the calculation are $I=100$ TW/cm^2 and $\Delta t_{\text{align}}=100$ fs, respectively.

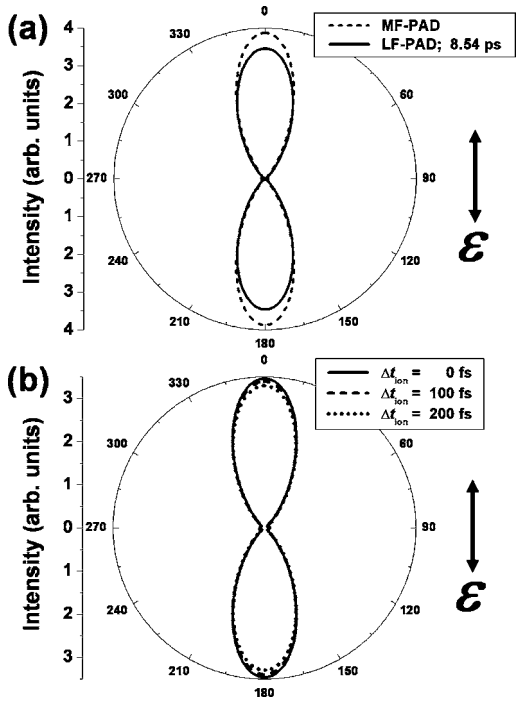

FIG. 11. (a) Polar plots of the calculated MF and LF PADs expected for the ionization of the a'' state. The LF PAD is calculated during the ionization of the ensemble with maximal alignment (at the delay time of 8.54 ps). (b) Effect of the ionization laser pulse width on the LF PADs. The polarization vector of the ionization light is parallel to that of the alignment laser light and is vertical in the plane of the figure. The initial rotational temperature of the sample is $T_{\text{R}}=20$ K. The intensity and pulse width of the alignment laser light in the calculation are $I=100$ TW/cm^2 and $\Delta t_{\text{align}}=100$ fs, respectively.

the ionization light with $\Delta t_{\text{align}}=0$, 100, and 200 fs are well fitted to the functions of $\cos^{26}\theta$, $\cos^{22}\theta$, and $\cos^{18}\theta$ with the angular widths of 24°, 27°, and 29° in FWHM, respectively. These widths are much narrower than that of the $\cos^4\theta$ distribution, 66°, which is generated by the two-photon excitation of the isotropic ensemble in the X state.

2. LF PAD in ionization from the aligned a'' state

The electronic state a'' is the $3s\sigma_{\text{g}}$ ($^1\Sigma_{\text{g}}^+$) member of the Rydberg series that converges to the ground electronic state of the cation. The Rydberg orbital, $4\sigma_{\text{g}}$ molecular orbital, has 94.22% s and 5.58% d characters [42] when it is approximated by one-center hydrogenic wave functions. In the ionization process of N_2^+ (X, $^2\Sigma_{\text{g}}^+$) $\leftarrow N_2$ (a'', $^1\Sigma_{\text{g}}^+$), if we truncate the partial wave expansion at $l \leqslant 3$, the selection rule allows only the $p\sigma$, $p\pi$, $f\sigma$, and $f\pi$ photoelectron partial waves.

Since the dynamical parameters of ionization have not been determined experimentally, we used the parameters that were obtained theoretically [42]. The magnitudes of the transition dipole matrix elements, $d_{l\lambda}$, have been calculated to be $d_{p\sigma}/d_{f\pi}=1.02$, $d_{p\pi}/d_{f\pi}=0.89$, and $d_{f\sigma}/d_{f\pi}=1.40$ for a photoelectron kinetic energy (PKE) of 2.8 eV. By considering the dominant s character of the $4\sigma_{\text{g}}$ orbital, an analogy with a hydrogenic atom would suggest that the contribution of the p component will be larger than that of f in the outgoing wave. However, in the *ab initio* calculations by Rijs *et al.* [42], the matrix elements $d_{f\sigma}$ and $d_{f\pi}$ of the f partial wave are always larger than $d_{p\sigma}$ and $d_{p\pi}$, respectively, for the PKE of 1–8 eV. On the other hand, no information on the phase shifts of the photoelectron partial waves is available in the literature. Therefore, we have considered the scattering phase shifts of the quantum defects of high Rydberg states. According to the multichannel quantum defect theory (MQDT) [43,44], the scattering phase shift, $\tau_{l\lambda}$, is related to the quantum defects of the Rydberg states, $\eta_{l\lambda}$, by $\tau_{l\lambda}=\pi\eta_{l\lambda}$, and can be extrapolated from the quantum defects of the high Rydberg states. The quantum defects of the p and f Rydberg series of N_2 have been determined by Jungen *et al.* from a detailed analysis of the near-threshold photoabsorption spectra [45]. They obtained $\eta_{p\sigma}=0.594$, $\eta_{p\pi}=0.672$, $\eta_{f\sigma}=0.036$, and $\eta_{f\pi}=0.035$ in radians. In our analysis, we used $\tau_{l\lambda}$ at $\mathcal{E}_{\text{PKE}}=2.8$ eV obtained from these $\eta_{l\lambda}$ values. The dynamical parameters of ionization are listed in Table I. We also assumed that $\tau_{l\lambda}$ at $\mathcal{E}_{\text{PKE}}=2.8$ eV is similar to those in the high

Rydberg states: the energy dependence of the dynamical phase shift was assumed to be negligible.

Figure 11(a) shows the polar plots of the calculated MF and LF PADs obtained for (2+1) REMPI via the a'' state. The LF PAD is calculated for the ionization of the maximally aligned ensemble (at the delay time of 8.54 ps). Both distributions are strongly peaked along the laser polarization and have no nodal patterns. Figure 11(b) shows the effect of the ionization pulse width on the LF PADs. Although a slightly weaker anisotropy of the LF PAD was obtained by the longer pulse width, in this particular case, the feature of the distribution does not change dramatically.

IV. CONCLUSIONS

We studied the PAD in the laboratory frame that is expected for the ionization of molecules aligned by an intense femtosecond laser pulse. We considered two distinct processes of the dynamical alignment of molecules in the electronic ground state by nonperturbative interaction with an intense laser field (>10 TW/cm^2) and one-photon ionization or (2+1) REMPI of the aligned ensemble by perturbative interaction with a moderate laser field (>10 GW/cm^2). Numerical simulation of the axis alignment and photoionization of N_2 molecules demonstrated that the LF PAD expected for the ionization of laser-aligned molecules is largely similar to the MF PAD.

ACKNOWLEDGMENTS

This work was supported by a Grant-in-Aid from the Ministry of Education, Culture, Sports, Science and Technology of Japan (Grant Nos. 13127204 and 14204603) and the Japan Science and Technology Agency. M.T. would like to acknowledge the Special Postdoctoral Researchers Program of RIKEN.

[1] A. V. Golovin, Opt. Spectrosc. **71**, 933 (1991).
[2] P. A. Hatherly, J. Adachi, E. Shigemasa, and A. Yagishita, J. Phys. B **28**, 2643 (1995).
[3] F. Heiser, O. Geßner, J. Viefhaus, K. Wieliczek, R. Hentges, and U. Becker, Phys. Rev. Lett. **79**, 2435 (1997).
[4] P. Downie and I. Powis, Phys. Rev. Lett. **82**, 2864 (1999).
[5] J. A. Davies, R. E. Continetti, D. W. Chandler, and C. C. Hayden, Phys. Rev. Lett. **84**, 5983 (2000).
[6] A. Lafosse, M. Lebech, J. C. Brenot, P. M. Guyon, O. Jagutzki, L. Spielberger, M. Vervloet, J. C. Houver, and D. Dowek, Phys. Rev. Lett. **84**, 5987 (2000).
[7] B. Friedrich and D. Herschbach, Phys. Rev. Lett. **74**, 4623 (1995).
[8] B. Friedrich and D. Herschbach, J. Phys. Chem. **99**, 15686 (1995).
[9] W. Kim and P. M. Felker, J. Chem. Phys. **104**, 1147 (1996).
[10] W. Kim and P. M. Felker, J. Chem. Phys. **107**, 2193 (1997).
[11] W. Kim and P. M. Felker, J. Chem. Phys. **108**, 6763 (1998).
[12] S. Kaesdorf, G. Schönhense, and U. Heinzmann, Phys. Rev. Lett. **54**, 885 (1985).
[13] T. Seideman, Phys. Rev. Lett. **83**, 4971 (1999).
[14] D. Normand, L. A. Lompre, and C. Cornaggia, J. Phys. B **25**, L497 (1992).
[15] P. Dietrich, D. T. Strickland, M. Laberge, and P. B. Corkum, Phys. Rev. A **47**, 2305 (1993).
[16] E. Charron, A. Giusti-Suzor, and F. H. Mies, Phys. Rev. Lett. **75**, 2815 (1995).
[17] F. Rosca-Pruna and M. J. J. Vrakking, Phys. Rev. Lett. **87**, 153902 (2001).
[18] F. Rosca-Pruna and M. J. J. Vrakking, J. Chem. Phys. **116**, 6567 (2002).
[19] F. Rosca-Pruna and M. J. J. Vrakking, J. Chem. Phys. **116**, 6579 (2002).
[20] I. V. Litvinyuk, K. F. Lee, P. W. Dooley, D. M. Rayner, D. M. Villeneuve, and P. B. Corkum, Phys. Rev. Lett. **90**, 233003 (2003).
[21] P. W. Dooley, I. V. Litvinyuk, K. F. Lee, D. M. Rayner, M. Spanner, D. M. Villeneuve, and P. B. Corkum, Phys. Rev. A **68**, 023406 (2003).
[22] S. C. Althorpe and T. Seideman, J. Chem. Phys. **110**, 147 (1999).
[23] G. Granucci, M. Persico, and P. Van Leuven, J. Chem. Phys. **120**, 7438 (2004).
[24] J. Ortigoso, M. Rodríguez, M. Gupta, and B. Friedrich, J. Chem. Phys. **110**, 3870 (1999).
[25] M. S. Child, Mol. Phys. **101**, 637 (2003).
[26] M. Comstock, V. Senekerimyan, and M. Dantus, J. Phys. Chem. A **107**, 8271 (2003).
[27] M. D. Poulsen, E. Péronne, H. Stapelfeldt, C. Z. Bisgaard, S. S. Viftrup, E. Hamilton, and T. Seideman, J. Chem. Phys. **121**, 783 (2004).
[28] I. Sh. Averbukh and R. Arvieu, Phys. Rev. Lett. **87**, 163601 (2001).
[29] P. Van Leuven, M. Malvaldi, and M. Persico, J. Chem. Phys. **116**, 538 (2002).
[30] M. Hippler, Mol. Phys. **97**, 105 (1999).
[31] R. G. Bray and R. M. Hochstrasser, Mol. Phys. **31**, 1199 (1976).
[32] D. Dill, J. Chem. Phys. **65**, 1130 (1976).
[33] J. G. Underwood and K. L. Reid, J. Chem. Phys. **113**, 1067 (2000).
[34] R. N. Zare, *Angular Momentum: Understanding Spatial Aspects in Chemistry and Physics* (John Wiley & Sons, New York, 1988).
[35] K. L. Reid and J. G. Underwood, J. Chem. Phys. **112**, 3643 (2000).
[36] K. P. Huber and G. Herzberg (data prepared by J. W. Gallagher and R. D. Johnson III), in "*NIST Chemistry WebBook*," *NIST Standard Reference Database Number 69*, edited by P. J. Linstrom and W. G. Mallard (National Institute of Standards and Technology, Gaithersburg, 2001).
[37] J. O. Hirschfelder, C. F. Curtis, and R. B. Bird, *Molecular Theory of Gases and Liquids* (Wiley, New York, 1954).
[38] G. Herzberg, *Molecular Spectra and Molecular Structure I: Spectra of Diatomic Molecules* (Van Nostrand Reinhold, New York, 1950).

[39] S. Motoki, J. Adachi, K. Ito, K. Ishii, K. Soejima, A. Yagishita, S. K. Semenov, and N. A. Cherepkov, Phys. Rev. Lett. **88**, 063003 (2002).
[40] S. Motoki, J. Adachi, K. Ito, K. Ishii, K. Soejima, A. Yagishita, S. K. Semenov, and N. A. Cherepkov, J. Phys. B **35**, 3801 (2002).
[41] T. F. Hanisco and A. C. Kummel, J. Phys. Chem. **95**, 8565 (1991).
[42] A. M. Rijs, E. H. G. Backus, C. A. de Lange, M. H. M. Janssen, K. Wang, and V. McKoy, J. Chem. Phys. **114**, 9413 (2001).
[43] M. J. Seaton, Rep. Prog. Phys. **46**, 167 (1983).
[44] C. H. Greene and Ch. Jungen, Adv. At. Mol. Phys. **21**, 51 (1985).
[45] Ch. Jungen, K. P. Huber, M. Jungen and G. Stark, J. Chem. Phys. **118**, 4517 (2003).